rigidly held planar geometry of PAMs promotes cooperative, $\pi-\pi$ interactions among several pairs of aromatic rings in neighboring molecules. Consequently, weak interactions between a single pair of aromatic rings that may be difficult to observe in small molecules are amplified by the PAM molecular architecture.[16] Because our synthetic chemistry allows aromatic functionalities to be varied easily, PAMs should provide a unique opportunity to study substituent effects on π-stacking interactions.

K_{assoc} was also found to vary significantly with temperature. According to van't Hoff analyses, $\Delta H = -5.0 \pm 0.2$ kcal mol^{-1} and $\Delta S = -9.2 \pm 0.8$ cal mol^{-1} K^{-1}. Surprisingly, PAM **2**, with alternating alkoxyl and ester groups, was found to have a smaller dimerization constant than **1** at 20 °C ($K_{assoc} = 18$ M^{-1}). Further studies give $\Delta H = -5.6 \pm 0.3$ kcal mol^{-1} and $\Delta S = -13.6 \pm 1.0$ cal mol^{-1} K^{-1} for the self-association of **2**. These results suggest that donor–acceptor interactions between alkoxyl and ester groups slightly favor π-stacking enthalpically, but disfavor π-stacking entropically relative to **1**. Overall, the entropy effect dominates near ambient temperature, resulting in a decrease in K_{assoc} for **2**. The difference in ΔS might also indicate that the dimer pair of **2** is more highly ordered than that of **1**. For **3**, which has segregated alkoxyl and ester groups, it was found that $K_{assoc} = 26$ M^{-1}, $\Delta H = -5.1 \pm 0.3$ kcal mol^{-1}, and $\Delta S = -10.8 \pm 1.0$ cal mol^{-1} K^{-1}. It is interesting to note that ΔS for dimerization of **1**, **2**, and **3** does not correlate with their symmetry, but may be rationalized by considerations of the shape of electrostatic potential surface of the dimer pair. Preliminary calculations based on the Hunter–Sanders model[18] suggest a face-to-face geometry with a 30° rotational off-set around the principal axis for the dimer of **1**.

No evidence of self-association was observed for **4** or **5**. The chemical shifts of the aromatic protons of these PAMs remain essentially constant with concentration and temperature. This clearly shows that aromatic substituents have a strong influence on the π-stacking interaction. We have also attempted to study the heteroassociation of **1** and **4** as well as **1** and **5** by NMR titration. We were unable to obtain accurate values of these heteroassociation constants because of the strong self-association of **1**. Qualitatively, however, the heteroassociation appears not to dominate over self-association of **1**. All of these data are consistent with the model developed by Hunter and Sanders.[18] Their model predicts that $\pi-\pi$ interactions between two π-deficient aromatic systems can be more favorable than those between a π-deficient and π-rich system or two π-rich systems.

In conclusion, we have demonstrated that PAMs are valuable models for studying the influence of chemical structure on $\pi-\pi$ interactions. We hope to use this information to design modular building blocks that can engage in specific noncovalent bonding for the rational construction of molecular materials.

Acknowledgment. Acknowledgment is made to the National Science Foundation for support through Grant CHE-9202095 and the NSF Young Investigator Program (1992–1997). J.S.M. thanks the 3M company for support through their nontenured faculty awards program. We thank Professor John Wiseman for comments and suggestions.

Supplementary Material Available: Listings of characterization data of compounds **1–5**, graphs and tables of variable-temperature ^{1}H NMR data,[17] and data analysis (17 pages). Ordering information is given on any current masthead page.

(16) The well-defined geometry seems essential for observing aggregation of these PAMs. This is supported by the fact that the open-chain oligomeric precursors to these macrocycles do not self-associate under the same conditions. Molecular modeling shows that hexa(PAM)s prefer to adopt a planar geometry. This is another example of Cram's preorganization.

(17) Variable-temperature ^{1}H NMR was done on a Bruker AM-360 equipped with a Eurotherm temperature controller. The temperature was calibrated with 4% methanol in methanol-d_4. All NMR spectra were taken in $CDCl_3$ with the residual solvent peak as the reference. $CDCl_3$ was assumed to expand linearly with temperature and have the same expansion coefficient as $CHCl_3$: *International Critical Tables of Numerical Data: Physics, Chemistry and Technology*; Washburn, E. W., Ed.; MacGraw-Hill: New York, 1928; Vol. III, p 27.

Direct Electron Transfer Involving Free-Solute Ferrocene in Fluid Electrolyte on an Oxocuprate (Bi(Pb) 2223) Electrode in the Superconducting State

S. J. Green, D. R. Rosseinsky,* and M. J. Toohey

Department of Chemistry
University of Exeter
Exeter EX4 4QD, U.K

Received July 17, 1992

High critical temperatures T_c invite the probing of the electronic spectra of superconducting oxocuprates by electrochemical study of charge transfer at the superconductor/electrolyte interface. Hitherto solid electrolytes[1,2] or frozen aqueous glasses[3,4] have been employed, the latter involving irresolvably complex proton reductions[3] or poorly-resolved $Fe^{II/III}$ processes.[4] Electron transfer effected between a superconducting electrode and free electroactive species in a fluid solution offers a wider choice of systems and more intimate electrode/electrolyte contact.[5] R. W. Murray et al.,[4-9] having developed low-temperature electrolytes and oxocuprate microelectrodes (on which low currents i minimize large iR potential drops through high electrolyte resistances R at ~100 K), now employ silver-coated oxocuprate macroelectrodes[10] (with proximity-effect Ag superconduction) bearing surface-bound electroactive species.

Following experimental advances i–v, we can now report free-solute ferrocene electrochemistry in fluid electrolyte at 102–104 K (i.e., $<T_c$) on superconducting Bi(Pb) 2223 oxocuprate itself ($Pb_{0.34}Bi_{1.84}Sr_{1.91}Ca_{2.03}Cu_{3.06}O_x$), T_c being established as 105 K by four-probe resistivity measurements.

(i) A new $<T_c$ solvent (cf. ref 5), of mixed chloroethane/tetrahydrofuran plus $LiBF_4$ background electrolyte, remains a supercooled glass retaining sufficient fluidity to allow significant diffusion at the electrode for >10 min.

(ii) Epoxy-embedded microelectrode fabrication from a wholly encapsulated sample[8] has been improved using partial encapsulation, thus. A ~5-mm-long wedge-shaped fragment, cut from a pressed oxocuprate pellet, is attached to copper wire at its rear edge with Ag paint and sanded to a point with fine emery paper. By standing this construction on its tip in a cylindrical PTFE mold subsequently filled with a cryorobust resin, only the extremity is exposed to provide the electrode surface.

(iii) A four-electrode resistance probe used as the electrical connection to the oxocuprate allows observation of the normal-to-superconducting transition prior to experimentation, and its reverse afterward. Thermal equilibrium at $<T_c$ (demonstrated by steady thermocouple and sample resistance readings) is rapidly restored (<10 min) after electrolyte injection (item v below), thermal perturbations being minimized by the large thermal mass of the cell.

(1) Pinkowski, A.; Jüttner, K.; Lorenz, W. J.; Saemann-Ischenko, G.; Breiter, M. W. *J. Electroanal. Chem.* **1990**, *286*, 253–256.
(2) Pinkowski, A.; Jüttner, K.; Lorenz, W. J. *J. Electroanal. Chem.* **1990**, *287*, 203–213.
(3) Bockris, J. O'M.; Wass, J. *J. Electroanal. Chem.* **1989**, *267*, 329–332.
(4) McDevitt, J. T.; Longmire, M.; Gollmar, R.; Jernigan, J. C.; Dalton, E. F.; McCarley, R.; Murray, R. W. *J. Electroanal. Chem.* **1988**, *243*, 465–474.
(5) Ching, S.; McDevitt, J. T.; Peck, S. R.; Murray, R. W. *J. Electrochem. Soc.* **1991**, *138*, 2308–2315.
(6) McDevitt, J. T.; McCarley, R. L.; Dalton, E. F.; Gollmar, R.; Murray, R. W.; Collman, J.; Yee, G. T.; Little, W. A. In *Chemistry of High Temperature Superconductors II*; Nelson, D. L., George, T. F., Eds.; ACS Symposium Series; 377, American Chemical Society: Washington, DC, 1988.
(7) McDevitt, J. T.; Ching, S.; Sullivan, M.; Murray, R. W. *J. Am. Chem. Soc.* **1989**, *111*, 4528–4529.
(8) Gollmar, R. O.; McDevitt, J. T.; Murray, R. W.; Collman, J. P.; Yee, G. T.; Little, W. A. *J. Electrochem. Soc.* **1989**, *136*, 3696–3701.
(9) McDevitt, J. T.; Murray, R. W.; Shah, S. I. *J. Electrochem. Soc.* **1991**, *138*, 1346–1350.
(10) Peck, S. R.; Curtin, L. S.; Tender, L. M. F.; Richardson, J. W.; Murray, R. W. *J. Electrochem. Soc.* **1992**, *139*, 170C (Abstract 434, Electrochemistry of High Temperature Superconductors, Electrochemical Society 181st Meeting, 20 May 1992).

0002-7863/92/1514-9702$03.00/0

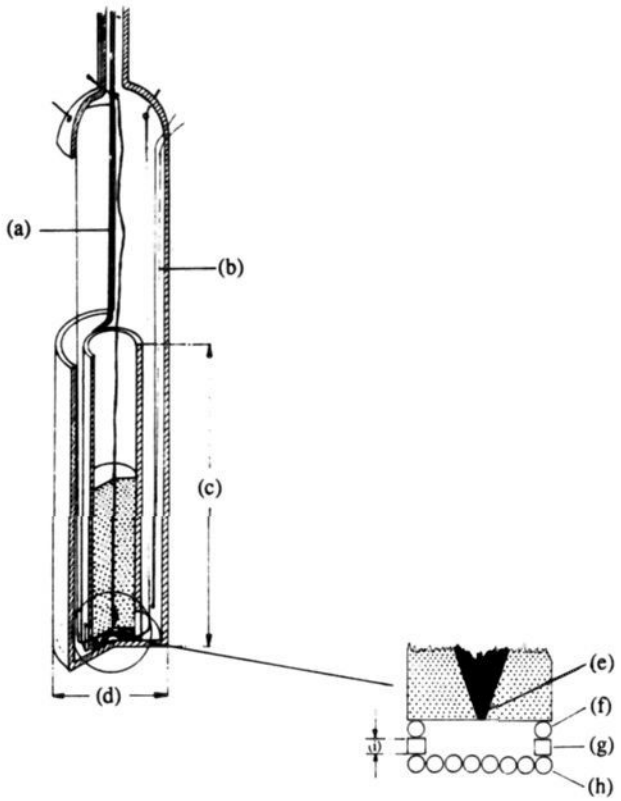

Figure 1. The cryoelectrochemistry cell with (inset) detail of resistance-minimizing electrode configuration: (a) syringe needle; (b) thermocouple; (c) 29 mm; (d) 16 mm; (e) working electrode; (f) Pt wire ring counter electrode; (g) PTFE spacing ring; (h) Ag wire spiral quasi-reference electrode; (i) 1 mm.

(iv) A resistance-minimizing[11] electrode configuration (Figure 1) was built into the cryoelectrochemistry cell, with temperature/atmosphere control by a nitrogen-cooled Oxford Instruments continuous-flow CF200 cryostat.

(v) Cell and electrode were precooled to $<T_c$ before injection of (ice-cold) electrolyte plus electroactive solution via a rubber septum cap and syringe needle (Figure 1). Electrode porosity effects,[4] appearing as excessive capacitative charging currents, are thereby obviated: while coming into contact with the oxocuprate surface, the incipiently vitrifying solution is too viscous to penetrate pores. Without our rapid cooling procedure, any defined charge-transfer current is lost. (Plugging the pores with encapsulating resin[8] is precluded here by the high mixed viscosity of the cryorobust resin.)

The results, repeated several times, are represented in Figure 2 as a cyclic voltammogram.[12] The zero-current steady-state Fc $\rightleftarrows$ $Fc^+ + e^-$ on the superconductor surface is perturbed by the varied applied potential, hence net charge transfer ($Fc \rightarrow Fc^+ + e^-$ in the forward abc limb and $Fc^+ + e^- \rightarrow Fc$ in the reverse cde limb) observable as current in the external circuit. The charge-transfer current (maintained by diffusion of electroactive species toward the electrode down the concentration gradient created by the surface reaction) is superimposed on the capacitative charging current (dashed lines) always attending potential changes at a charged interface. The peaked response is attributable to the slow diffusion at 102 K, while the large peak separation (1.5 V) implies considerable solution resistance. After >10 min, nucleation and subsequent freezing (visible through the optical-measurement windows of the cryostat) occur with a loss of electrochemical current.

(11) Van Duyne, R. P.; Reilly, C. N. *Anal. Chem.* **1972**, *44*, 142–152.
(12) Bard, A. J.; Faulkner, L. R. *Electrochemical Methods*; John Wiley and Sons: New York, 1980.

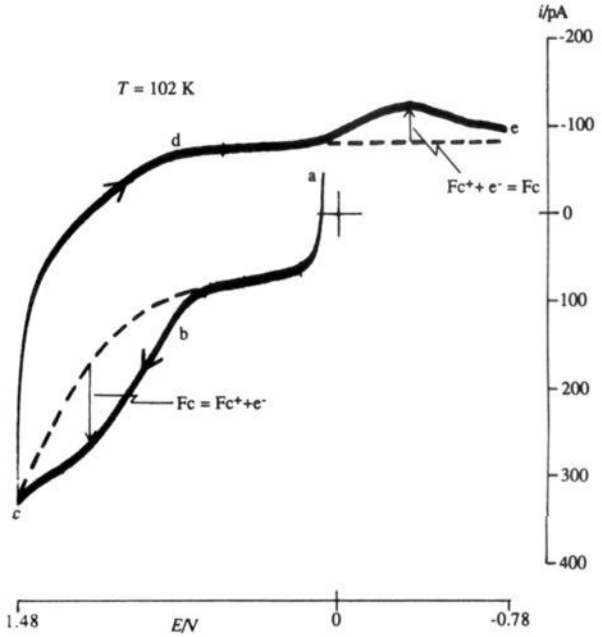

Figure 2. Cyclic voltammogram of 5 mM ferrocene in 0.6 M $LiBF_4$/2:1 volume-ratio chloroethane:tetrahydrofuran on a Bi(Pb) 2223 superconducting microelectrode at 102 K: scan rate, 10 mV s^{-1}; *E*, potential of superconducting surface relative to the Ag wire quasi-reference electrode; *i*, current observed between oxocuprate and Pt; – – –, capacitative background current.

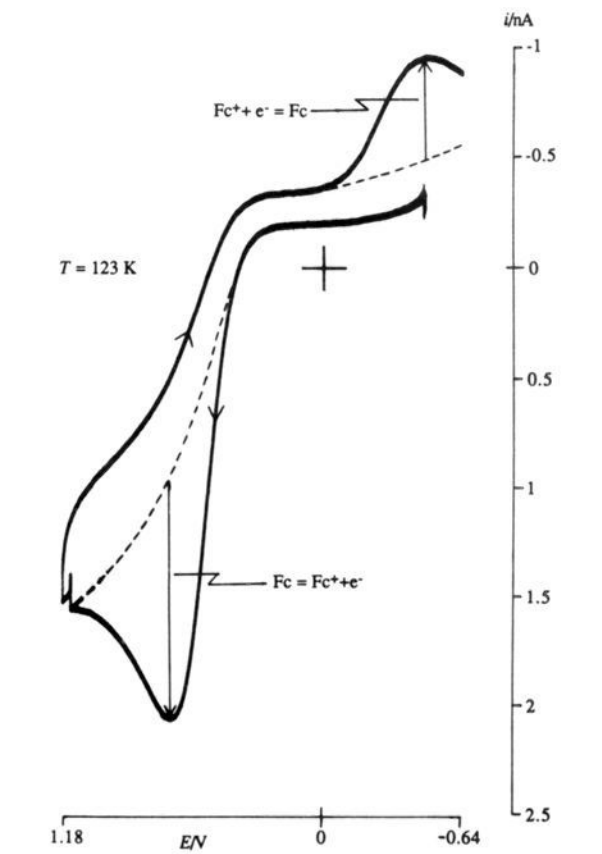

Figure 3. Cyclic voltammogram of 5 mM ferrocene/electrolyte as in Figure 2 on a Bi(Pb) 2223 microelectrode at 123 K.

Thus the operability of the system is demonstrated and presages the possibilities of (i) obtaining kinetic parameters from impedance; (ii) using other electroactive species, with,[10] e.g., Tl 2223 oxocuprate superconducting at 128 K,[13] where our method pro-

duces excellent results (Figure 3) with no electrolyte freezing apparent; (iii) testing Kuznetsov's prediction[14] regarding two-electron processes; and (iv) possible in-situ composition modification at *below* T_c by, e.g., electrochemical Li^+ intercalation, already established[15] as a room temperature process modifying subsequent superconducting behavior.

Acknowledgment. We thank Merck Ltd. and the SERC for funding and Merck Ltd. for materials.

(13) Liu, R. S.; Tallon, J. L.; Edwards, P. P. *Physica C* **1991**, *182*, 119-122.
(14) Kuznetsov, A. M. *J. Electroanal. Chem.* **1990**, *278*, 1-15.
(15) Fleischer, N. A.; Manassen, J. *J. Electrochem. Soc.* **1992**, *139*, 170C (Abstract 437, Electrochemistry of High Temperature Superconductors, Electrochemical Society 181st Meeting, 20 May 1992).

Fluorimetric Chemodosimetry. Mercury(II) and Silver(I) Indication in Water via Enhanced Fluorescence Signaling

Mi-Young Chae and Anthony W. Czarnik*

Department of Chemistry
The Ohio State University
Columbus, Ohio 43210

Received April 10, 1992

Fluoroionophores chemically communicate ion concentrations and have been the subject of substantial investigation in aqueous metal ion analysis.[1] For example, salicylidene-*o*-aminophenol, itself nonfluorescent at pH 4.5, forms a yellow-green fluorescent complex with Al(III).[2] However, the vast majority of fluoroionophores signal metal ions via fluorescence quenching (CHEQ) rather than fluorescence enhancement (CHEF).[3] We have observed that anthrylazamacrocycles display CHEF toward Zn(II) and Cd(II) in water, but CHEQ toward all other complexing transition metals, including Hg(II).[4] In fact, there are no reported examples of fluoroionophores that indicate Hg(II) with selectivity, much less with fluorescence enhancement. Because enhancement methods offer sensitivity advantages, mechanisms that signal inherently quenching metals via increasing emission are of interest. Furthermore, novel signal transduction mechanisms also may provide the selectivities unrelated to binding equilibria required for practical ion discrimination in water.[5] We now report the synthesis of a fluorimetric dosimeter[6] that indicates Hg(II), a strongly quenching ion, with fluorescence enhancement in aqueous solution.

Because Hg(II) is a thiophilic metal ion, sulfur-based intramolecular quenching functional groups were considered. While thioethers do quench anthracene fluorescence by photoinduced electron transfer (PET), that process is not as efficient as quenching by amines.[7] Thus, we chose the thioamide group (**1**);

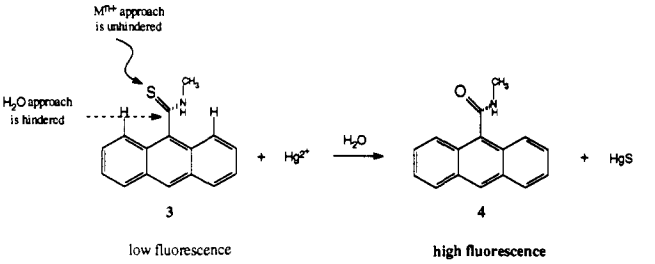

Figure 1.

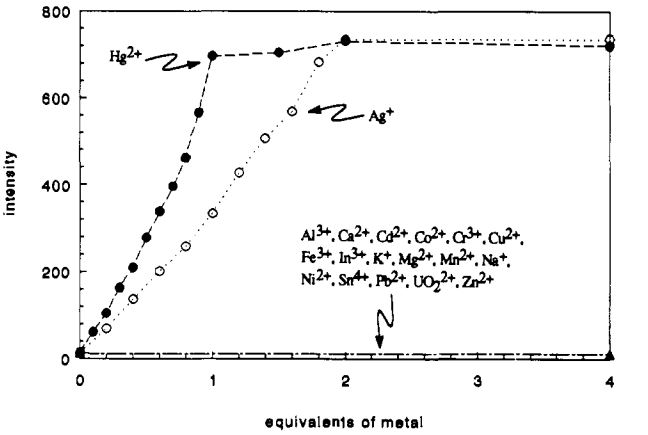

Figure 2. Fluorescence metal titrations of **3**. Solutions are 23 μM **3** in 0.01 M HEPES buffer, pH 7. Measurements shown were made after 70 h, principally to demonstrate the stability of **3** toward nonindicating metals. The Hg(II) reaction is 87% complete and the Ag(I) reaction 73% complete after 10 min under stoichiometric conditions and at room temperature.

because the C=S double bond is weak, resonance structure **2** is the dominant resonance contributor.[8] Thiolates are in general

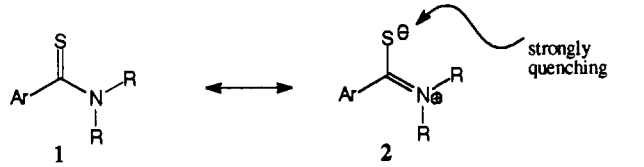

readily oxidized, which suggested that the thioamide group might be a strong intramolecular quenching entity. 9-[(Methylamino)thiocarbonyl]anthracene (**3**) was obtained as a red-brown solid (mp 183-184 °C dec) by Lawesson's reagent thiation of carboxamide **4**.[9] Compound **3** demonstrates fluorescence at 413.5 nm 56 times less intense than that of *N*-methyl-9-anthracenecarboxamide (**4**), consistent with the prediction.

As shown in Figure 2, Hg(II) and Ag(I) additions uniquely result in fluorescence enhancements in nearly direct proportion to their stoichiometries; the signal increase after complete reaction is 55-fold. Al(III), Ca(II), Cd(II), Co(II), Cr(III), Cu(II), Fe(III), In(III), K(I), Mg(II), Mn(II), Na(I), Ni(II), Pb(II), Sn(IV), UO_2(II), and Zn(II) yield no change in emission intensity under identical conditions. The observed stoichiometries, 1:1 for Hg(II) and 2:1 for Ag(I), are as predicted by the signal transduction mechanism shown in Figure 1. Both ions effect the desulfurization of **3**, yielding anthryl amide **4** and the insoluble metal sulfides as products. Because the amide group does not efficiently quench fluorescence, and (importantly) because it does not complex metals in aqueous solution, the conversion of **3** to **4** results in a net fluorescence enhancement with linear and

(1) (a) West, T. S. *Complexometry with EDTA and Related Reagents*; BDH: New York, NY, 1969; especially pp 65-73. (b) Seitz, W. R. In *Fiber Optic Chemical Sensors and Biosensors*; Wolfbeis, O. S., Ed.; CRC Press: Boca Raton, FL, 1991; Vol. II, pp 4-6. (c) Czarnik, A. W. In *Frontiers in Supramolecular Organic Chemistry and Photochemistry*; Schneider, H.-J., Durr, H., Eds., VCH: New York, 1991; pp 109-122.
(2) Holzbecher, Z. *Chem. Listy* **1958**, *52*, 1822.
(3) The acronyms CHEF (chelation-enhanced fluorescence) and CHEQ (chelation-enhanced quenching) have been used to characterize the phenomenological responses of complexation-induced fluorescence increase or decrease, respectively.
(4) Akkaya, E. U.; Huston, M. E.; Czarnik, A. W. *J. Am. Chem. Soc.* **1990**, *112*, 3590.
(5) We have reported previously an example of chelatoselective fluorescence perturbation that provides such secondary selectivity: Huston, M. E.; Czarnik, A. W. *J. Am. Chem. Soc.* **1990**, *112*, 7054.
(6) Following the terminology of Wolfbeis, dosimeters are designed for cumulative assay, in contrast to sensors, which give real-time data and are reversible: Wolfbeis, O. S. In *Fiber Optic Chemical Sensors and Biosensors*; Wolfbeis, O. S., Ed.; CRC Press: Boca Raton, FL, 1991; Vol. I, p 2.
(7) Private communication, J. Toner, Sterling Drug Company.
(8) Duus, F. In *Comprehensive Organic Chemistry*; Pergamon Press: Oxford, 1979; Vol. 3, p 440.
(9) We synthesized **3** from 9-anthracenecarboxylic acid by conversion to the acid chloride, reaction with methylamine, and thiation with Lawesson's reagent. Full synthetic and characterization details are available as supplementary material.

0002-7863/92/1514-9704$03.00/0